J. Fluid Mech. (2010), *vol.* 651, *pp.* 319–337.
doi:10.1017/S0022112009993946

Structural sensitivity of the secondary instability in the wake of a circular cylinder

FLAVIO GIANNETTI[1]†, SIMONE CAMARRI[2] AND PAOLO LUCHINI[1]

[1]Dipartimento di Ingegneria Meccanica, Università di Salerno, Via Ponte Don MeLillo 1, 84084 Fisciano (SA), Italy

[2]Dipartimento di Ingegneria Aerospaziale, Università di Pisa, Via G. Caruso 8, 56122 Pisa, Italy

(Received 29 April 2009; revised 11 December 2009; accepted 14 December 2009; first published online 26 March 2010)

The sensitivity of the three-dimensional secondary instability of a circular-cylinder wake to a structural perturbation of the associated linear equations is investigated. In particular, for a given flow condition, the region of maximum coupling between the velocity components is localized by using the most unstable Floquet mode and its adjoint mode. The variation of this region in time is also found by considering a structural perturbation which is impulsively applied in time at a given phase of the vortex-shedding process. The analysis is carried out for both mode A and mode B types of transition in the wake of a circular cylinder using a finite-difference code. The resulting regions identified as the core of the instability are in full agreement with the results reported in the literature and with the *a posteriori* checks documented here.

1. Introduction

The secondary instability in the wake of a circular cylinder has been widely investigated in the literature using both experiments and numerical simulations (see for instance Barkley & Henderson 1996 and Williamson 1996*b* for a review). Among the different approaches used to study the transition process, linear stability analysis plays a fundamental role since it can provide a great deal of insights into the instability mechanism. The first global three-dimensional stability analysis of the periodic wake behind a circular cylinder was performed by Noack, König & Eckelmann (1993) and Noack & Eckelmann (1994) who used a Galerkin projection method to represent both the base flow and the perturbation. Despite the reduced number of retained ad hoc basis functions, they were able to capture the main features of the transition process observed in the experimental investigations. Successively, Barkley & Henderson (1996) performed a highly accurate Floquet stability analysis using a spectral element method. They predict that at a Reynolds number (based on the cylinder diameter and on the free-stream velocity) $Re \simeq 189$, the two-dimensional von Kármán street becomes linearly unstable to three-dimensional perturbations. The Floquet analysis shows the existence of two separate bands of synchronous unstable modes: the first one (mode A) appears for $Re > 189$ and is characterized by a spanwise wavelength of about 4 cylinder diameters, whereas the second one (mode B) develops for $Re > 259$ and has a shorter spanwise wavelength (about 1 diameter). The results of the linear stability

† Email address for correspondence: fgiannetti@unisa.it

analysis are consistent with the experimental flow visualizations of Williamson (1988) and with other direct numerical simulations documented in the literature (see for example Karniadakis & Triantafyllou 1992; Mittal & Balachandar 1995 and Zhang, Fey & Noack 1995). In a real flow, the transition for mode B occurs at a lower Reynolds number (see Williamson 1988) than that predicted by a linear analysis, because the development of mode A substantially alters the assumed two-dimensional base flow. As a result, at $Re \approx 230$–240, the wake already shows the evidence of both modes and of their nonlinear interactions.

Different interpretations (see for instance Thompson, Leweke & Williamson 2001) have been given in order to explain the physical nature of the secondary instability of the cylinder wake, which is not completely understood yet. Independently of the physical origin of this transition, Barkley (2005) has recently shown that 'small regions of the full flow just behind the cylinder are responsible for the linear instabilities despite the fact that the actual linear modes extend many cylinder diameters downstream the cylinder'. This observation has two implications. First of all, this is important information that might be used in formulating an interpretation of the physical nature of the secondary instability in the cylinder wake. Secondly, shorter computational domains can be used for the linear stability analysis leading to reduced computational costs. A similar behaviour was also observed for the first instability of the cylinder wake by Giannetti & Luchini (2007). In the context of a genuine two-dimensional analysis, introducing a concept similar to that of 'wavemaker' used in the asymptotic theory of global modes (see for example Chomaz 2005), they determined where in space a localized structural perturbation of the linearized Navier–Stokes operator produces the largest drift of the unstable eigenvalue. In such a way, by inspecting the spatial characteristics of the product between the associated direct and the adjoint eigenfunctions, they were able to locate the core of the global instability which gives rise to the Kármán vortex street; the analysis reveals that the 'wavemaker' (i.e. the core of the instability) is localized in the rear part of the separation bubble.

In the present work, the approach adopted by Giannetti & Luchini (2007) for localizing the core of the vortex-shedding instability is generalized to the case in which the base flow is time-periodic. In particular, the sensitivity of the Floquet exponent to a generic structural perturbation of the linearized equations is carried out by evaluating both the direct and the adjoint eigenfunctions of the Floquet transition operator. When a time-constant localized structural perturbation is considered, a spatial sensitivity map is built in order to identify precisely the region of the flow where the instability arises. The dependence of the sensitivity map on the phase of the vortex shedding is also found by considering a structural perturbation which is impulsively applied in time at a given phase of the vortex-shedding process. The resulting theory is finally applied in order to identify the core of the linear three-dimensional instability in the wake of a circular cylinder in the two types of linear transition, modes A and B. As shown in the paper, the sensitivity maps found are in full agreement with what was observed heuristically by Barkley (2005), and show that the instability is highly localized.

2. Problem formulation

The flow around an infinitely long circular cylinder positioned with its axis orthogonal to the incoming uniform flow is considered. The flow is described using a Cartesian coordinate system, with the z axis coinciding with the cylinder axis and the x axis aligned with the flow direction. The fluid motion can be described by

the unsteady incompressible Navier–Stokes equations, which are made dimensionless using the cylinder diameter D^* as the characteristic length scale, the velocity of the incoming uniform stream U^*_∞ as the reference velocity and the (constant) fluid density ρ^*:

$$\frac{\partial \boldsymbol{U}}{\partial t} + \boldsymbol{U}\cdot\nabla\boldsymbol{U} = -\nabla P + \frac{1}{Re}\Delta\boldsymbol{U}, \tag{2.1a}$$

$$\nabla\cdot\boldsymbol{U} = 0, \tag{2.1b}$$

where $\boldsymbol{U}$ is the velocity vector with components $\boldsymbol{U}=(U, V, W)$, P is the reduced pressure and $Re = U^*_\infty D^*/\nu^*$ is the Reynolds number (ν^* being the kinematic viscosity of the fluid). As for the boundary conditions, no-slip and no-penetration conditions are applied on the cylinder surface Γ_c, and the flow is assumed to asymptotically approach the incoming uniform stream in the far field.

2.1. *Floquet analysis*

It is well known that at $Re > Re_{c1} \approx 47$, a time-periodic vortex shedding develops in the wake of the cylinder and the flow remains periodic and two-dimensional ($W=0$) for $Re_{c1} < Re < Re_{c2} \approx 189$. The linear stability analysis to three-dimensional disturbances of the two-dimensional time-periodic base flow is carried out using Floquet theory (Drazin 2002). This approach was used for the first time in the study of the secondary instability of the cylinder wake by Noack *et al.* (1993). Following the classical approach, the total flow field $\boldsymbol{Q}=\{\boldsymbol{U}, P\}$ is decomposed into the sum of a two-dimensional time-periodic base flow $(\boldsymbol{U}_b, P_b)$ of period T, which is a solution of the two-dimensional case (x–y plane) of the Navier–Stokes equations (2.1), and a small unsteady perturbation:

$$\boldsymbol{U}(x, y, z, t) = \boldsymbol{U}_b(x, y, t) + \epsilon\,\frac{1}{\sqrt{2\pi}}\int_{-\infty}^{\infty}\boldsymbol{u}(x, y, k, t)\,\exp(\mathrm{i}kz)\,\mathrm{d}k, \tag{2.2a}$$

$$P(x, y, z, t) = P_b(x, y, t) + \epsilon\,\frac{1}{\sqrt{2\pi}}\int_{-\infty}^{\infty}p(x, y, k, t)\,\exp(\mathrm{i}kz)\,\mathrm{d}k, \tag{2.2b}$$

where ϵ is the disturbance amplitude, and $\boldsymbol{u}$ and p are the Fourier-transformed velocity and pressure disturbances in the spanwise direction, which is a homogeneous direction for the base flow. Introducing (2.2) in (2.1) and linearizing in ϵ, we obtain two problems describing the evolution of the two-dimensional periodic base flow and the dynamics of the three-dimensional perturbations. In particular, the base flow is governed by the two-dimensional version of (2.1), whereas the perturbed field is described by the three-dimensional unsteady linearized Navier–Stokes equations (LNSEs). When the Fourier transform in the z direction is applied to the LNSEs, the following set of equations is obtained for each wavenumber k

$$\frac{\partial \boldsymbol{u}}{\partial t} + L_k\{\boldsymbol{U}_b, Re\}\boldsymbol{u} + \nabla_k p = \boldsymbol{0}, \tag{2.3a}$$

$$\nabla_k\cdot\boldsymbol{u} = 0, \tag{2.3b}$$

where $\nabla_k \equiv ((\partial/\partial x), (\partial/\partial x), (\mathrm{i}k))$ is the Fourier-transformed gradient operator, L_k stands for the Fourier-transformed linearized Navier–Stokes operator:

$$L_k\{\boldsymbol{U}_b, Re\}\boldsymbol{u} = \boldsymbol{U}_b\cdot\nabla_k\boldsymbol{u} + \boldsymbol{u}\cdot\nabla_k\boldsymbol{U}_b - \frac{1}{Re}\Delta_k\boldsymbol{u} \tag{2.4}$$

and $\Delta_k \equiv \nabla_k\cdot\nabla_k$ is the Fourier-transformed Laplacian operator. In the Floquet stability analysis, the linearized flow field $\boldsymbol{q} = \{\boldsymbol{u}, p\}$ is further assumed to have

the following form

$$\boldsymbol{q}(x, y, k, t) = \hat{\boldsymbol{q}}(x, y, k, t)\exp(\sigma t), \tag{2.5}$$

where σ is the Floquet exponent while $\hat{\boldsymbol{q}} = \{\hat{\boldsymbol{u}}, \hat{p}\}$ is a non-trivial periodic field, with the same period T as the base flow. Using (2.3), we easily verify that $\hat{\boldsymbol{q}}$ satisfies the following set of equations

$$\frac{\partial \hat{\boldsymbol{u}}}{\partial t} + \sigma\hat{\boldsymbol{u}} + L_k\{\boldsymbol{U}_b, Re\}\hat{\boldsymbol{u}} + \nabla_k\hat{p} = \boldsymbol{0}, \tag{2.6a}$$

$$\nabla_k \cdot \hat{\boldsymbol{u}} = 0. \tag{2.6b}$$

These are supplemented with homogeneous boundary conditions on the cylinder surface and appropriate far-field radiation conditions. This means that far enough from the cylinder the perturbation behaves locally as an outgoing plane wave. While this last requirement enforces the correct causality relation, it does not generally imply that the disturbance vanishes at infinity. For the cylinder case, however, the spreading of the wake with the resulting attenuation of the vorticity and the rapid decay of the outer potential field produce a reduction of the perturbation amplitude with the radial distance. Thus, in our case, the far-field conditions may be formulated as

$$\hat{\boldsymbol{q}} = \{\hat{\boldsymbol{u}}, \hat{p}\} \;\rightarrow\; \{\boldsymbol{0}, 0\} \qquad \text{as} \quad r \rightarrow \infty. \tag{2.7}$$

The system of (2.6) along with the above boundary conditions and the periodicity requirement for the solution represents an eigenvalue problem for σ. The Floquet multipliers μ, which are the eigenvalues of the Floquet transition operator, are related to the Floquet exponents σ by the expression $\mu = \exp(\sigma T)$. By inspecting expression (2.5), it is therefore easy to realize that the base flow becomes unstable whenever there exists a Floquet multiplier $\mu > 1$ or equivalently a Floquet exponent $\sigma > 0$.

2.2. *Adjoint equations*

In order to gain a better understanding of the secondary instability mechanism, we will make use of the properties of adjoint operators. The adjoint of the LNSEs (2.3) is defined using the generalized Lagrange identity (Ince 1926). For any pair of suitably differentiable fields $\boldsymbol{q} \equiv \{\boldsymbol{u}, p\}$ and $\boldsymbol{g}^+ \equiv \{\boldsymbol{f}^+, m^+\}$, which do not necessarily have to satisfy (2.3), the following Lagrange identity is constructed using differentiation by parts

$$\begin{aligned}
&\left[\left(\frac{\partial \boldsymbol{u}}{\partial t} + L_k\{\boldsymbol{U}_b, Re\}\boldsymbol{u} + \nabla_k p\right)\cdot \boldsymbol{f}^+ + (\nabla_k\cdot\boldsymbol{u})\;\hat{m}^+\right] \\
&\quad + \left[\boldsymbol{u}\cdot\left(\frac{\partial \boldsymbol{f}^+}{\partial t} + L_k^+\{\boldsymbol{U}_b, Re\}\boldsymbol{f}^+ + \nabla_k m^+\right) + p(\nabla_k\cdot\boldsymbol{f}^+)\right] \\
&\quad = \frac{\partial \boldsymbol{u}\cdot\boldsymbol{f}^+}{\partial t} + \nabla_k\cdot\boldsymbol{J}(\boldsymbol{q}, \boldsymbol{g}^+),
\end{aligned} \tag{2.8}$$

where $\boldsymbol{J}(\boldsymbol{q}, \boldsymbol{g}^+)$ is the 'bilinear concomitant'

$$\boldsymbol{J}(\boldsymbol{q}, \boldsymbol{g}^+) = \boldsymbol{U}_b(\boldsymbol{u}\cdot\boldsymbol{f}^+) + \frac{1}{Re}(\nabla_k\boldsymbol{f}^+\cdot\boldsymbol{u} - \nabla_k\boldsymbol{u}\cdot\boldsymbol{f}^+) + m^+\boldsymbol{u} + p\boldsymbol{f}^+ \tag{2.9}$$

and L_k^+ is the adjoint linearized Navier–Stokes operator

$$L_k^+\{\boldsymbol{U}_b, Re\}\boldsymbol{f}^+ = \boldsymbol{U}_b\cdot\nabla_k\boldsymbol{f}^+ - \nabla_k\boldsymbol{U}_b\cdot\boldsymbol{f}^+ + \frac{1}{Re}\Delta_k\boldsymbol{f}^+. \tag{2.10}$$

Examining the second term in the square brackets on the left-hand side of the Lagrange identity (2.8), we define the adjoint equations as

$$\frac{\partial \boldsymbol{f}^+}{\partial t} + L_k^+\{\boldsymbol{U}_b, Re\}\boldsymbol{f}^+ + \nabla_k m^+ = \boldsymbol{0}, \tag{2.11a}$$

$$\nabla_k \cdot \boldsymbol{f}^+ = 0. \tag{2.11b}$$

In this paper, we are interested in the Floquet adjoint modes; in particular, if $\boldsymbol{q}(x, y, k, t) = \hat{\boldsymbol{q}}(x, y, k, t)\exp(\sigma t)$ is the Floquet mode of the LNSEs corresponding to the Floquet exponent σ, we define its adjoint as the solution of the adjoint LNSEs (2.11) of the form $\boldsymbol{g}^+(x, y, k, t) = \hat{\boldsymbol{g}}^+(x, y, k, t)\exp(-\sigma t)$. Here $\hat{\boldsymbol{g}}^+ = \{\hat{\boldsymbol{f}}^+, \hat{m}^+\}$ is a periodic field (with the same period T as the base flow) which satisfies the eigenvalue problem defined by the following set of equations

$$\frac{\partial \hat{\boldsymbol{f}}^+}{\partial t} - \sigma\,\hat{\boldsymbol{f}}^+ + L_k^+\{\boldsymbol{U}_b, Re\}\hat{\boldsymbol{f}}^+ + \nabla_k \hat{m}^+ = \boldsymbol{0}, \tag{2.12a}$$

$$\nabla_k \cdot \hat{\boldsymbol{f}}^+ = 0, \tag{2.12b}$$

together with homogeneous boundary conditions on the cylinder surface and appropriate radiation conditions in the far field. As for the direct mode, this does not generally mean that the adjoint field has to vanish as the radial distance $r \to \infty$. However, in our case, the particular structure of the base flow leads to a rapid decay of the adjoint mode, so that the far-field conditions become

$$\hat{\boldsymbol{g}}^+ = \{\hat{\boldsymbol{f}}^+, \hat{m}^+\} \;\to\; \{\boldsymbol{0}, 0\} \qquad \text{as} \quad r \to \infty. \tag{2.13}$$

The adjoint solution can be used to study the receptivity of the Floquet mode to an external forcing. More precisely, the receptivity of the mode to a periodic forcing in the momentum and/or continuity equation is proportional to the local magnitude of the adjoint fields $\hat{\boldsymbol{f}}^+$ and $\hat{m}^+$.

3. Receptivity to spatially localized feedbacks

The stability and receptivity analysis of the two-dimensional periodic wake, although it can provide useful information on the instability characteristics and on the response of the forced system, is not able to locate the regions of the flow where the secondary instability mechanism acts. For this reason, in this paper, we generalize to time-periodic base flows the approach first introduced by Giannetti & Luchini (2007) to study the first instability of the cylinder wake. In particular, using a similar procedure, a structural stability analysis of the Floquet problem is carried out in order to determine the region of the flow field in which the instability mechanism arises; if this region is localized in space, we will denote it as the 'core' of the instability.

Let us therefore consider the perturbed Floquet problem

$$\frac{\partial \hat{\boldsymbol{u}}'}{\partial t} + \sigma'\hat{\boldsymbol{u}}' + L_k\{\boldsymbol{U}_b, Re\}\hat{\boldsymbol{u}}' + \nabla_k \hat{p}' = \delta H(\hat{\boldsymbol{u}}', \hat{p}'), \tag{3.1a}$$

$$\nabla_k \cdot \hat{\boldsymbol{u}}' = \delta R(\hat{\boldsymbol{u}}', \hat{p}'), \tag{3.1b}$$

in which δH and δR denote two generic linear differential operators expressing the structural perturbation of the original differential problem. If the structural perturbation is small, the solution $\hat{\boldsymbol{q}}'(x, y, k, t)\exp(\sigma' t)$ of the perturbed problem

(3.1) can be expanded in a neighbourhood of the solution $\hat{\boldsymbol{q}}(x, y, k, t)\exp(\sigma t)$ of the unperturbed problem ($\delta H(\hat{\boldsymbol{u}}', \hat{p}') = \boldsymbol{0}$ and $\delta R(\hat{\boldsymbol{u}}', \hat{p}') = 0$). In particular, (i) taking

$$\hat{\boldsymbol{u}}' = \hat{\boldsymbol{u}} + \delta\hat{\boldsymbol{u}}, \tag{3.2}$$

$$\hat{p}' = \hat{p} + \delta\hat{p}, \tag{3.3}$$

where $\delta\hat{\boldsymbol{u}}$ and $\delta\hat{p}$ denote small corrections of the velocity and pressure fields, respectively, due to the structural perturbation, (ii) expanding the perturbed Floquet exponent σ' as

$$\sigma' = \sigma + \delta\sigma, \tag{3.4}$$

(iii) inserting in (3.1) and (iv) neglecting quadratic terms, we obtain the following differential problem for the Floquet exponent drift

$$\frac{\partial\delta\hat{\boldsymbol{u}}}{\partial t} + \sigma\delta\hat{\boldsymbol{u}} + L_k\{\boldsymbol{U}_b, Re\}\delta\hat{\boldsymbol{u}} + \nabla_k\delta\hat{p} = -\delta\sigma\hat{\boldsymbol{u}} + \delta H(\hat{\boldsymbol{u}}, \hat{p}), \tag{3.5a}$$

$$\nabla_k \cdot \delta\hat{\boldsymbol{u}} = \delta R(\hat{\boldsymbol{u}}, \hat{p}). \tag{3.5b}$$

Multiplying (3.5) by $\exp(\sigma t)$ and, in analogy with (2.5), defining $\delta\boldsymbol{q}(x, y, k, t) = \delta\hat{\boldsymbol{q}}(x, y, k, t)\exp(\sigma t)$, we can rewrite the previous equations as

$$\frac{\partial\delta\boldsymbol{u}}{\partial t} + L_k\{\boldsymbol{U}_b, Re\}\delta\boldsymbol{u} + \nabla_k\delta p = -\delta\sigma\boldsymbol{u} + \delta H(\boldsymbol{u}, p), \tag{3.6a}$$

$$\nabla_k \cdot \delta\boldsymbol{u} = \delta R(\boldsymbol{u}, p). \tag{3.6b}$$

Applying the Lagrange identity (2.8) to the field $\delta\boldsymbol{q}$ and the adjoint Floquet mode $\boldsymbol{g}^+(x, y, k, t) = \hat{\boldsymbol{g}}^+(x, y, k, t)\exp(-\sigma t)$ corresponding to the unperturbed eigenvalue σ, integrating in time over the period T and in space over the whole flow domain $\mathscr{D}$, the following identity is obtained

$$\begin{aligned}
&\int_t^{t+T}\int_{\mathscr{D}}\left[\left(\frac{\partial\delta\boldsymbol{u}}{\partial t} + L_k\{\boldsymbol{U}_b, Re\}\delta\boldsymbol{u} + \nabla_k\delta p\right)\cdot\boldsymbol{f}^+ + (\nabla_k\cdot\delta\boldsymbol{u})\,\hat{m}^+\right]\mathrm{d}S\,\mathrm{d}t \\
&\quad + \int_t^{t+T}\int_{\mathscr{D}}\left[\delta\boldsymbol{u}\cdot\left(\frac{\partial\boldsymbol{f}^+}{\partial t} + L_k^+\{\boldsymbol{U}_b, Re\}\boldsymbol{f}^+ + \nabla_k m^+\right) + \delta p\ (\nabla_k\cdot\boldsymbol{f}^+)\right]\mathrm{d}S\,\mathrm{d}t \\
&= \int_t^{t+T}\int_{\mathscr{D}}\frac{\partial\delta\boldsymbol{u}\cdot\boldsymbol{f}^+}{\partial t}\,\mathrm{d}S\,\mathrm{d}t \;+\; \int_t^{t+T}\oint_{\partial\mathscr{D}}\boldsymbol{J}(\delta\boldsymbol{q}, \boldsymbol{g}^+)\cdot\boldsymbol{n}\,\mathrm{d}l\,\mathrm{d}t.
\end{aligned} \tag{3.7}$$

Assuming that both the adjoint and the direct modes vanish in the far field and using the periodicity in time of $\delta\hat{\boldsymbol{u}}$ and $\hat{\boldsymbol{f}}^+$, it is straightforward to verify that the right-hand side of identity (3.7) is zero. Lastly, using the fact that the adjoint mode satisfies (2.12) and using (3.5), the drift $\delta\sigma$ of the Floquet exponent due to the structural perturbation can be expressed as

$$\delta\sigma = \frac{\displaystyle\int_t^{t+T}\int_D \boldsymbol{f}^+\cdot\delta H(\boldsymbol{u}, p) + m^+\,\delta R(\boldsymbol{u}, p)\,\mathrm{d}S\,\mathrm{d}t}{\displaystyle\int_t^{t+T}\int_{\mathscr{D}}\boldsymbol{f}^+\cdot\boldsymbol{u}\,\mathrm{d}S\,\mathrm{d}t}. \tag{3.8}$$

Equation (3.8) is valid for a generic structural perturbation; the associated shift in the Floquet exponent can be precisely calculated once the operators δH and δR are specified. Equation (3.8) can be simplified if we consider structural perturbations that are localized in space. In particular, as in the work of Giannetti & Luchini (2007), here we confine our attention to spatially localized feedback from

force to velocity; thus the perturbation in the mass-conservation equation is not considered ($\delta R = 0$), whereas the operator $\delta H(\boldsymbol{u}, p)$ is assumed to have the following form

$$\delta H(\boldsymbol{u}, p) = \delta(x - x_0, y - y_0)\ \boldsymbol{C}_0 \cdot \boldsymbol{u}, \tag{3.9}$$

where $\boldsymbol{C}_0$ is a generic constant (feedback) matrix, (x_0, y_0) are the coordinates of the point where the feedback acts and, $\delta(x - x_0, y - y_0)$ denotes the Dirac delta function. Such a feedback might be physically produced by introducing an infinitesimal small device in the flow field which exerts a force on the fluid whose direction and strength depend on the local value of the disturbance velocity. In this case, however, the physical presence of the small device would not only act at the perturbation level but would also produce a shift of the eigenvalue by modifying the unsteady base flow on which the instability analysis is carried over. The Floquet multipliers, in fact, can be influenced in two different ways: by a structural perturbation force depending on the small velocity fluctuations alone (and therefore acting only on the linearized equations) or by a force responding to the unsteady base flow which directly modifies the structure of the nonlinear two-dimensional unsteady Navier–Stokes equations. Both analyses can be performed making use of the adjoint equations and serve for different purposes. The structural perturbation acting only on the linearized equations is the appropriate tool to study the position of the 'wavemaker' and investigate the physical nature of the instability, whereas the second analysis is more appropriate to develop effective control strategies to suppress the instability or for a direct comparison with the experiments. Sensitivity analyses based on a similar framework have been used in the past to evaluate the effect of base-flow variation on the stability properties of parallel flows (Bottaro, Corbett & Luchini 2003), boundary layers (Zuccher, Luchini & Bottaro 2004) and bluff-body wakes (see for example Marquet, Sipp & Jacquin 2008; Marquet *et al.* 2009 and Luchini, Giannetti & Pralits 2008).

In this paper, however, we are only interested in identifying the region where the instability mechanism takes place, so that we focus on the effects of structural perturbations acting only on the linearized equations. Substituting (3.9) in (3.8), we obtain:

$$\delta\sigma = \frac{\displaystyle\int_t^{t+T}\int_D \boldsymbol{f}^+ \cdot \delta(x - x_0, y - y_0)\ \boldsymbol{C}_0 \cdot \boldsymbol{u}\,\mathrm{d}S\,\mathrm{d}t}{\displaystyle\int_t^{t+T}\int_{\mathscr{D}} \boldsymbol{f}^+ \cdot \boldsymbol{u}\,\mathrm{d}S\,\mathrm{d}t} = \boldsymbol{C}_0 : S(x_0, y_0, k), \tag{3.10}$$

where S is the sensitivity tensor of the Floquet mode defined as

$$S(x, y, k) = \frac{\displaystyle\int_t^{t+T} \boldsymbol{f}^+(x, y, k, t)\ \boldsymbol{u}(x, y, k, t)\,\mathrm{d}t}{\displaystyle\int_t^{t+T}\int_{\mathscr{D}} \boldsymbol{f}^+ \cdot \boldsymbol{u}\,\mathrm{d}S\,\mathrm{d}t}. \tag{3.11}$$

Note that this definition is independent of the particular feedback process (which is defined only through the entries of the matrix $\boldsymbol{C}_0$). Thus expression (3.11) can be used to better understand the effects of a generic force-velocity coupling which is localized in space. Important information pertaining the feedback mechanism can be easily retrieved by inspecting the different components of the sensitivity tensor. A more concise way to extract information from S is to choose a norm and build

a spatial sensitivity map by plotting at each point in space the value $||S(x, y, k)||$. Different norms can be used for this purpose, depending on the type of feedback we are interested in. Here we use the spectral norm in order to produce a spatial map representing the sensitivity of the Floquet exponent to a force-velocity feedback in which the force is oriented in the worst possible direction. By looking at this map, it is possible to locate the regions of the flow where the structural perturbation produces the largest eigenvalue drift.

Phase information in the structural sensitivity can be recovered by considering a structural perturbation which is impulsively applied in time at a precise phase of the periodic base flow, corresponding to time t_0

$$\delta H(\boldsymbol{u}, p) = \delta((t \bmod T) - t_0))\, \delta(x - x_0, y - y_0)\, \boldsymbol{C}_0 \cdot \boldsymbol{u}. \tag{3.12}$$

In this case, the variation of the Floquet exponent σ is given by

$$\delta\sigma = \boldsymbol{C}_0 : I(x_0, y_0, t_0, k), \tag{3.13}$$

where I is the instantaneous sensitivity tensor defined by

$$I(x, y, t, k) = \frac{\boldsymbol{f}^+(x, y, k, t)\boldsymbol{u}(x, y, k, t)}{\displaystyle\int_t^{t+T} \int_{\mathscr{D}} \boldsymbol{f}^+ \cdot \boldsymbol{u}\, \mathrm{d}S\, \mathrm{d}t}. \tag{3.14}$$

4. Results and discussion

4.1. *Numerical approach*

The two-dimensional incompressible Navier–Stokes equations (2.1), their linearized version describing the evolution of the three-dimensional disturbances (2.3) and the corresponding adjoint equations (2.11) are discretized in conservative form on a staggered smoothly varying Cartesian mesh by using a standard second-order-accurate finite-difference scheme. The cylinder surface is simulated by an immersed-boundary technique that preserves the second-order accuracy of the discretization (see Giannetti & Luchini 2007 for details). For the simulation of the two-dimensional base flow, a constant streamwise velocity profile ($U = 1$, $V = 0$) is imposed both at the inflow and at the side boundaries, while convective type boundary conditions are applied on the outflow boundary ($\partial V/\partial x = 0$ and $-P + 2/Re\,\partial U/\partial x = 0$). For the simulation of the linearized equations, the perturbation velocity field is assumed to vanish at the inflow and at the side boundaries, while convective conditions are applied on the outflow boundary ($\partial v/\partial x = 0$, $\partial w/\partial x = 0$ and $-p + 2/Re\ \partial u/\partial x = 0$). The resulting semi-discrete equations are advanced in time by the hybrid third-order Runge–Kutta/Crank–Nicolson scheme of Rai & Moin (1991). The diffusive terms and the pressure field are treated implicitly while the convective terms are discretized explicitly. Thus, at each temporal sub-step, a Stokes-type operator is solved by inverting directly the resulting linear system through the use of a sparse LU factorization (the software package UMFPACK by Davis 2004 is used for this purpose). Lastly, the discrete adjoint equations are obtained by taking the adjoint of the discretized linearized equations; this is achieved in practice by deriving the adjoint of each subroutine which compose the code for solving the LNSEs and reversing the original calling order. In this way, the boundary conditions for the discrete adjoint equations are automatically taken into account in the discretization. Both the direct and the adjoint dominant Floquet modes are then numerically extracted with a

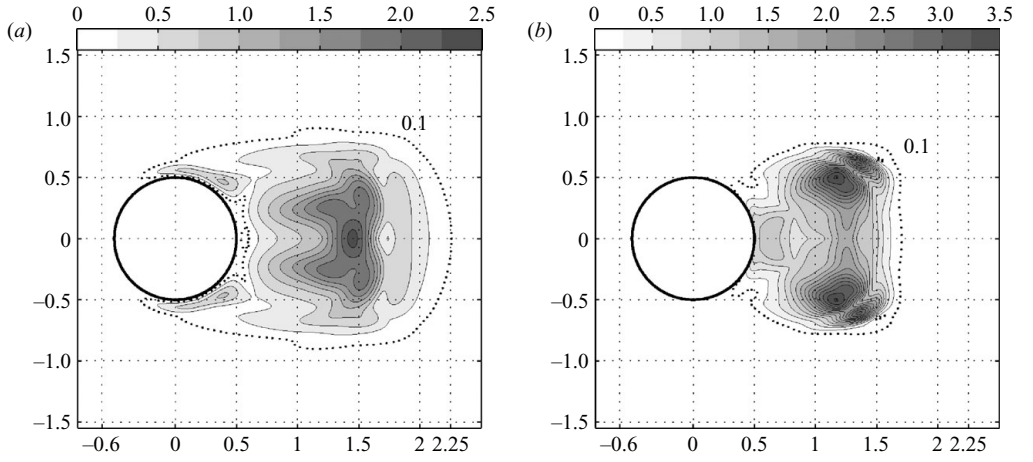

FIGURE 1. Spectral norm of the tensor field S at each point of the domain for (a) mode A ($Re = 190$, $k = 1.585$) and (b) mode B ($Re = 260$, $k = 7.64$)

classical power iteration; the equations are marched in time (the adjoint backwards in time) until the dominant mode emerges. As a further check, the same eigenvalue problem was also solved making use of the ARPACK library (Lehoucq, Sorensen & Yang 1998). As expected, since we solve the adjoint of the discrete equations, the Floquet multipliers for the direct and adjoint problems coincide to machine precision. The results documented in the present work have been obtained using a rectangular computational domain; the inflow, outflow and lateral boundaries are located at a distance from the cylinder axis equal to $L_i = 16.5\ D$, $L_o = 34.5\ D$ and $L_h = 11\ D$, respectively. According to the convergence tests documented by Barkley & Henderson (1996), the selected domain size leads to sufficiently accurate results for the purposes of the present work. For instance in Barkley (2005), a work which is also dedicated to test the sensitivity of the Floquet multipliers to the size of the computational domain, accurate results are obtained with an even smaller domain ($L_i = 8\ D$, $L_o = 25\ D$ and $L_h = 8\ D$). In order to achieve a better resolution close to the cylinder surface, a non-uniform grid is used for the computations, globally made of 600 (350) nodes in the x (y) direction. The grid spacing in the x (y) direction varies from $1.5 \cdot 10^{-2}\ D$ ($1.5 \cdot 10^{-2}\ D$) on the cylinder to $1.5 \cdot 10^{-1}\ D$ ($2.4 \cdot 10^{-1}\ D$) at the outflow boundary. For the temporal discretization, a non-dimensional time step $\Delta t\ U_\infty / D$ equal to 10^{-2} has been used, leading approximately to 510 (483) temporal steps for each shedding cycle at $Re = 190$ ($Re = 260$).

4.2. *Structural sensitivity results*

Two Reynolds numbers have been considered here, i.e. $Re = 190$ and $Re = 260$, to investigate mode A and mode B, respectively. The same couple of Reynolds numbers was used in Barkley (2005). In order to estimate the accuracy of the results obtained by our numerical procedure, we firstly compared the Strouhal number of the alternate vortex shedding in the base flow (i.e. its frequency in time normalized with U_∞^* and D^*) with the data available in the literature. At $Re = 190$ ($Re = 260$), a Strouhal number $St = 0.1971$ ($St = 0.2087$) has been obtained, a result in good agreement with the value $St = 0.1954$ ($St \simeq 0.2070$), extrapolated from figure 1 in Barkley & Henderson (1996), the percentage variation being approximately equal to 0.9 % (0.8 %). Following Barkley & Henderson (1996), at $Re = 190$ ($Re = 260$) the Floquet analysis has been

carried out by considering a wavenumber in the spanwise direction equal to $k = 1.585$ ($k = 7.64$), corresponding to a wavelength equal to 3.96 D (0.82 D), which for the Reynolds number considered is the most critical one for mode A (mode B). As expected, the considered configurations are extremely close to those of marginal stability, the resulting Floquet multiplier being equal to 1.002 (0.995). As a further validation of the Floquet analysis, the critical Reynolds number for the instability of Mode A (Mode B) has been searched by fixing the value of the spanwise wavenumber to the value mentioned above. As a result, we found a critical Reynolds number for the first appearance of Mode A (Mode B) approximately equal to $Re_1 \simeq 189.77$ ($Re_2 \simeq 260.21$), which is in agreement with $Re_1 = 188.5 \pm 1$ ($Re_2 = 259 \pm 2$) reported by Barkley & Henderson (1996).

After that the results for the base flow and the linear stability analysis were validated and the adjoint mode computed, the sensitivity to spatially localized feedback was calculated by using a discretization of (3.11), which is consistent with the temporal and spatial discretization used for the governing equations. As a first result, in figure 1, the spectral norm of the tensor field S (see (3.11)) is displayed for both Mode A and Mode B in the flow conditions specified above. According to (3.10), a localized structural perturbation affects the unstable modes only in those regions in which the tensor field S is significantly non-null. A different norm for the tensor S could have been used as well. For instance, we also tried the trace norm, and the maps obtained did not differ significantly from the ones reported here. Moreover, the sensitivity of the maps reported in figure 1 to variations of (a) the spanwise wavenumber (small variations), (b) the Reynolds number (small variations), (c) the grid resolution and (d) the computational domain size has been verified. Because no appreciable change of the results has been observed, we have not reported here the results of such tests for the sake of brevity.

It is interesting to note that the sensitivity tensor S vanishes almost everywhere except for a very localized region in the near-wake of the cylinder, for both mode A and mode B, indicating that the 'core' of the three-dimensional instability is sharply localized in space. This behaviour is similar to that which Giannetti & Luchini (2007) observed for the first instability of the cylinder wake. In that case, in fact, the sensitivity is localized in two lobes placed symmetrically across the separation bubble. In order to test our numerical results and verify that only that region where S is significantly different from zero are important for the instability mechanism, the Floquet stability analysis has been carried out in progressively smaller rectangular subdomains around that region. The considered base flow was always the one computed on the whole domain, and in restricting it to subdomains, the grid points were left unchanged in order to avoid interpolation procedures that might affect the results. The Floquet multipliers obtained in the subdomains are then compared to the reference ones obtained on the whole domain. The boundary conditions on each side of the subdomains are identical to the ones adopted in the corresponding side of the whole domain. The results of the test described above are reported for three representative subdomains in table 1, together with the results obtained in Barkley (2005), in which an identical experiment is carried out. Comparing the results reported in table 1 with the maps in figure 1 (some grid lines in the figure coincide with the boundaries of the considered subdomains in order to simplify the comparison), it is possible to confirm that the core of the three-dimensional instability is localized in those regions in which the tensor S is significantly different from zero. In particular, large variations of the Floquet multiplier are obtained only when the considered subdomain does not properly contain the region of high sensitivity shown in the

Source	L_i/D	L_o/D	L_h/D	Re	k	μ	$\Delta\mu$ (%)	Re	k	μ	$\Delta\mu$ (%)
Present	0.6	3.0	1.5	190	1.585	0.999	−0.3	260	7.64	0.996	0.1
Present	0.6	2.5	1.5	190	1.585	0.953	−4.9	260	7.64	0.996	0.1
Present	0.6	2.0	1.0	190	1.585	0.352	−64.9	260	7.64	1.003	0.80
Present	0.6	1.3	1.0	190	1.585	1.483	48.0	260	7.64	15.237	>1000
Barkley (2005)	0.0	3.0	1.5	190	1.6	1.030	0.3	260	7.5	1.049	1.4
Barkley (2005)	0.0	2.25	1.5	190	1.6	0.914	11.6	260	7.5	1.068	3.2
Barkley (2005)	0.0	1.5	1.5	190	1.6	0.490	52.6	260	7.5	not reported	>60

TABLE 1. Variations of the Floquet multipliers evaluated on subdomains; the reference values for mode A (mode B) are 1.002 (0.995) for the present work and 1.034 (1.035) for Barkley (2005); data from Barkley (2005) has been extracted from figure 2 of the referenced paper.

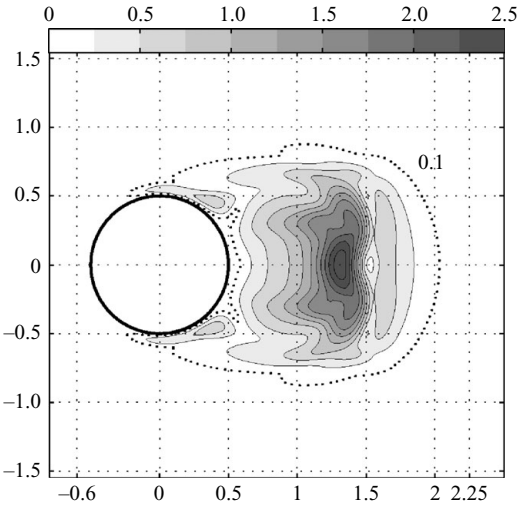

FIGURE 2. Spectral norm of the tensor field S for mode A ($k = 1.585$) evaluated at $Re = 260$.

maps of figure 1. Moreover, it is interesting to note that the maps obtained here are also in full agreement with the results reported in Barkley (2005). In particular, when the intermediate subdomain is used (see table 1, second last line), a significant variation of the Floquet multiplier associated to mode A is obtained, while the multiplier associated to mode B remains almost unchanged. This result agrees with the fact that the sensitivity region of mode A extends approximately $0.5\,D$ further downstream if compared to that of mode B, as indicated by the isoline corresponding to the value of the spectral norm of S equal to 0.1 plotted with a dotted line in figure 1. In particular, although the norm of S in the region of maximum sensitivity is larger for mode B than for mode A, at section $x = 2.25\ D$ the norm of S for mode B is between two and three orders of magnitude lower than the one corresponding to mode A.

As a general trend, for both mode A and mode B, when the Reynolds number is increased the regions of maximum sensitivity slightly shift closer to the cylinder surface. As an example, the sensitivity map for mode A at $Re = 260$ is presented in figure 2. Comparing with the results obtained at $Re = 190$, we can observe that not only the shape but also the values of the sensitivity remain essentially the same in the range of Reynolds numbers considered.

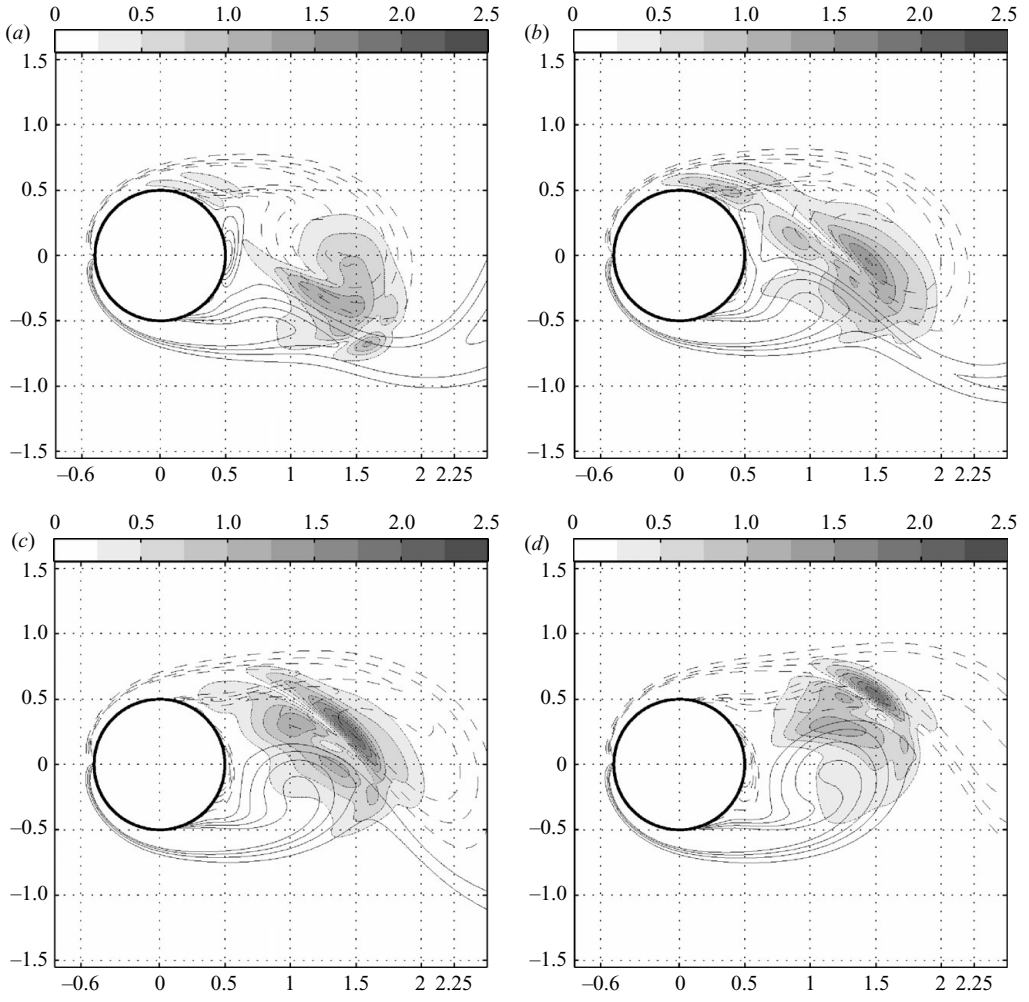

FIGURE 3. Mode A ($Re = 190$, $k = 1.585$): spectral norm of the tensor field I (grey-scale) and vorticity field of the base flow (levels going from -4 to 4 by steps of size equal to 1, negative contours being dashed) at (a–d) the four subsequent phases 0, $\pi/4$, $\pi/2$ and $3\pi/4$ among the eight in which the vortex-shedding cycle has been equally divided. The remaining phases can be recovered by symmetry.

The results summarized by the spatial maps in figures 1 (and 2) are obtained by evaluating the integral in expression (3.11) over a shedding cycle and therefore represents an average sensitivity over a period T. Although this contains sufficient information to locate precisely the core of the instability, it is also very interesting to visualize how the sensitivity varies in time during a vortex-shedding cycle. In order to recover the phase information, the instantaneous sensitivity tensor (3.14) has also been computed and its spectral norm is plotted for both mode A and mode B in figures 3 and 4, respectively. In both figures, four subsequent phases are considered among the eight in which the vortex-shedding cycle has been equally divided. More precisely, the pictures correspond to a phase angle of 0, $\pi/4$, $\pi/2$ and $3\pi/4$, respectively. The remaining phases can be easily recovered by symmetry. The comparison between the two figures shows that the regions where the norm of I is significant for the

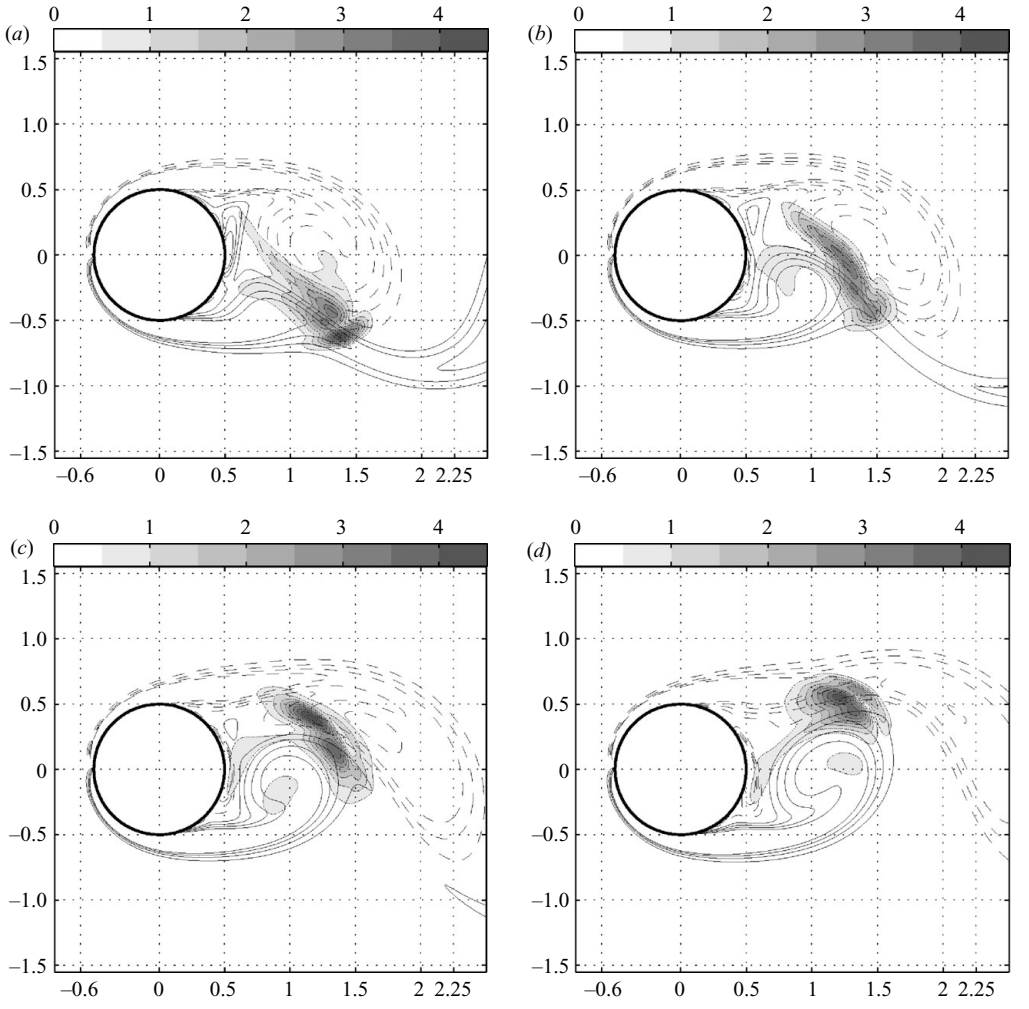

FIGURE 4. Mode B ($Re = 260$, $k = 7.64$): spectral norm of the tensor field I (grey-scale) and vorticity field of the base flow (levels going from -4 to 4 by steps of size equal to 1, negative contours being dashed) at (a–d) the four subsequent phases 0, $\pi/4$, $\pi/2$ and $3\pi/4$ among the eight in which the vortex-shedding cycle has been equally divided. The remaining phases can be recovered by symmetry. In this figure, the phases of the vortex shedding have been aligned with those reported in figure 3 for Mode A.

two unstable modes are approximately centred around the same region, i.e. the region separating the clockwise and counterclockwise vorticities originating from the lower and upper shear layers, respectively, although the map of mode B is definitely more concentrated around this region. Moreover, in both cases the tensor norm is not negligible in the vortex which is forming closest to the cylinder surface. As far as mode B is concerned, the sensitivity map is also different from zero in the neighbourhood of the downstream face of the cylinder. On the other hand, the map associated to mode A is more spread out and it extends close to the separation point on the lateral side which is opposite to the forming vortex closest to the cylinder surface. In both cases, however, the maximum sensitivity during the vortex-shedding cycle is reached in the regions where the maps in figure 1 show their maxima. In particular,

looking at the sensitivity maps, it is clear that the main difference between the results obtained for modes A and B is the location of the region of the maximum sensitivity. In fact, while for mode A the region of maximum is located across the symmetry line passing for the cylinder centre, for mode B the peaks are reached in two regions symmetrically placed with respect to the line $y = 0$, at a distance from it of about one cylinder radius. The fact that the core of the instability for modes A and B shows these differences might reflect the different nature of the instability mechanism which originates them. Concerning this point, despite the large number of experimental, theoretical and numerical investigations of the three-dimensional transition of the cylinder wake, the precise physical nature of the secondary instabilities is not fully understood yet and has generated much debate. Several possible mechanisms have been proposed in the past, ranging from elliptic instabilities of the forming vortex core for mode A (Williamson 1996*a*; Leweke & Williamson 1998) and hyperbolic instabilities of the braid regions between the rollers for mode B (Williamson 1996*a*), to centrifugal (Brede, Eckelmann & Rockwell 1996) or Benjamin–Feir (Leweke & Provansal 1995) type instabilities (see for instance Thompson *et al.* 2001 for a more detailed discussion). However, no rigorous or conclusive evidence was supplied to support any of these speculations. In such context, we believe that the present analysis could provide valuable information to gain a better understanding of the three-dimensional transition process and could offer new interesting perspectives to study the physical nature of the instability. In particular, the sensitivity maps described in this section could be helpful in identifying special features of the base flow which might be related to the spatial and temporal evolution of the instability and might be used to develop a new approach to the problem. As an example, in the Appendix, the existence of closed Lagrangian orbits in the wake of the cylinder is shown and their possible link with the secondary instability is shortly discussed.

5. Conclusions

In this paper, the secondary instability of the cylinder wake is investigated by performing a structural sensitivity analysis. To this purpose, the approach originally proposed by Giannetti & Luchini (2007) to investigate the first instability of the cylinder wake is generalized in order to include time-periodic base flows in the analysis. In particular, the sensitivity of the most unstable Floquet modes with respect to a localized force-velocity feedback is carried out. This type of structural perturbation allows the identification of the instability core by inspecting the spatial structure of the tensor product between the direct and the adjoint eigenfunctions associated with the most unstable three-dimensional mode. Such quantity takes into account the 'feedback' which is at the origin of the self-excited oscillation and is therefore useful to locate the region where the instability mechanism acts. Both constant-in-time and impulsive-in-time structural perturbations have been considered. The second type of feedback, in particular, has allowed to follow the spatial and temporal evolution of the instability core during the different phases of the vortex shedding.

The analysis described above has been carried out for mode A ($Re = 190$, $k = 1.585$) and mode B ($Re = 260$, $k = 7.64$) by using a finite-difference code. For each case, a sensitivity map is found which is associated to the constant-in-time structural perturbation. The two resulting maps, which are very localized in the near-wake region, are verified by performing stability analysis on progressively smaller subdomains containing the core of the instability, i.e. the region in space in which the sensitivity to the structural perturbation is significantly different from zero. As a result, the

variations of the resulting Floquet multiplier are appreciable only when the core of the instability is not properly included in the considered subdomain. The same type of tests are carried out by Barkley (2005) in order to find heuristically the core of the instability. The results of such tests are shown to be in full agreement with the maps found in the present paper. Analogous maps are found as a function of the phase of the vortex shedding when an impulsive-in-time structural perturbation is considered. In this way, the time evolution of the instability core has been uncovered and differences in the behaviour of mode A and mode B discussed. Such results might be very useful to gain a better understanding of the three-dimensional transition process and could offer new perspectives (see the Appendix) to study the physical nature of the instability, which is not completely understood yet.

We conclude by highlighting that the strategy proposed here to localize the secondary instability arising in the wake of a circular cylinder is a general approach and can be used to study a generic linear global instability superposed to a generic time-periodic base flow.

Appendix. Closed Lagrangian trajectories

The analysis performed in the present paper shows that the core of the secondary instability, for both mode A and mode B, is highly localized in space. A similar result was also observed by Giannetti & Luchini (2007) and Luchini *et al.* (2008) for the first instability of the cylinder wake. In that case, in fact, the core of the global instability (the 'wavemaker') is located in a region placed in the rear part of the separation bubble and approximately confined in the streamwise direction by the positions of the centres of the two counter-rotating vortices and the re-attachment point of the wake bubble. Such points are equilibrium points (or critical points) of the dynamical system

$$\frac{\mathrm{d}\boldsymbol{X}(t)}{\mathrm{d}t} = \boldsymbol{U}_b(\boldsymbol{X}(t), t), \tag{A 1}$$

describing the position $\boldsymbol{X}$ of a Lagrangian particle convected by the base flow $\boldsymbol{U}_b$. For Re larger than 47, the wake becomes globally unstable and a periodic vortex shedding sets in. In these conditions, no equilibrium points of (A 1) can be found. However, since the base flow is now periodic, there might exist particular Lagrangian points which evolve along closed orbits and return to their initial position after one period T. Such solutions are fixed points of the first 'return map' (or Poincaré map) associated with a specific phase of the shedding cycle. The closed orbits described by these Lagrangian particles can be thought of as a generalization of the three equilibrium points existing in the wake of the cylinder at low Reynolds numbers. As for the first instability, it seems therefore interesting to check if the core of the secondary instability evolves in times following the movement of these points or, more generally, if a visual correlation can be found between the regions of highest sensitivity and the closed Lagrangian orbits.

From a mathematical point of view, these closed path lines are the solutions of the ordinary differential equation (A 1) subject to the periodicity requirement

$$\boldsymbol{X}(t+T) = \boldsymbol{X}(t). \tag{A 2}$$

By numerically solving (A 1) and (A 2) with a fourth-order Runge–Kutta scheme coupled to a Newton–Raphson procedure, we were able to find three closed Lagrangian trajectories in the periodic wake of the circular cylinder. To our knowledge, this is the first time that such orbits have been displayed. For sake

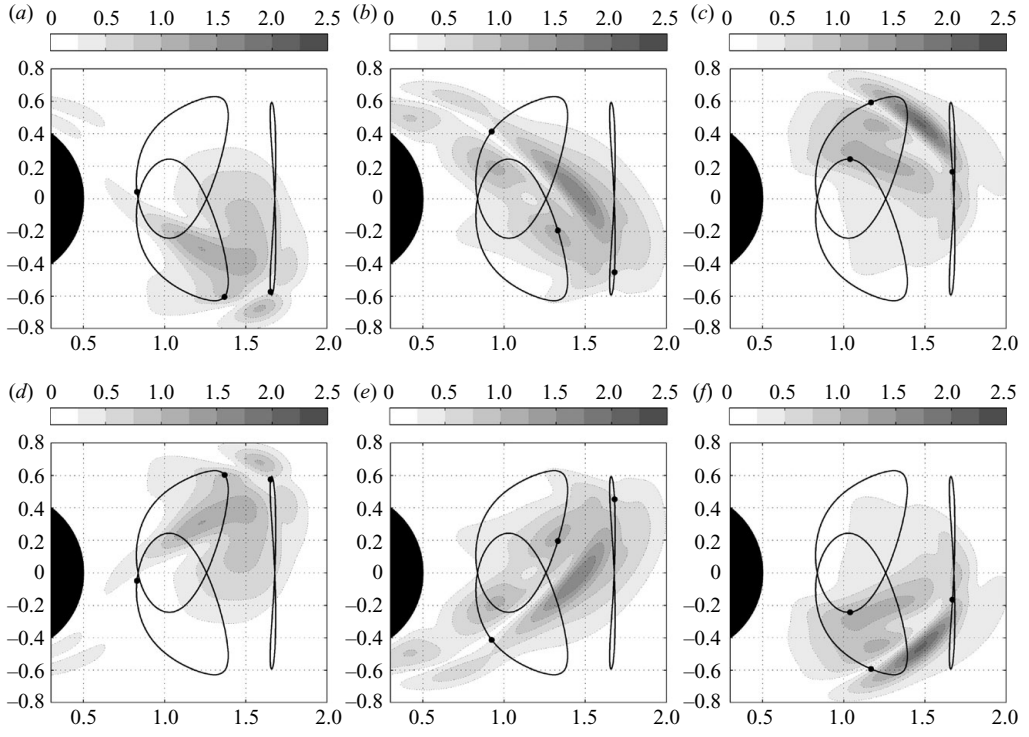

FIGURE 5. Closed Lagrangian trajectories of the periodic base flow at $Re = 190$: the movement of the points (small circles) along the closed orbits (black lines) is shown for (a–f) the six phases (0, $\pi/3$, $2\pi/3$, π, $4\pi/3$ and $5\pi/3$) in which the vortex-shedding cycle has been equally divided. The spectral norm of the sensitivity tensor $I(x, y, t)$ for mode A at $k = 1.585$) is also superposed in order to show the strong correlation existing among the orbits and the regions of instantaneous maximum sensitivity.

of precision, we have to say that orbits that close after more than one period may also exist, but we did not look for them, since they do not have the same periodicity as the unstable global modes.

Among the three closed orbits that we were able to find numerically, one is symmetric and the other two are symmetrically located with respect to $y = 0$. It is interesting to note that all the closed orbits are enclosed in the region of maximum sensitivity of modes A and B as given in figure 1. The movement of the material points (little circles) along the closed orbits (black line) during a whole shedding cycle is shown in figures 5 and 6, respectively, for $Re = 190$ and $Re = 260$. In both cases, the entire period has been divided into 6 equal intervals. In order to better show the correlation existing between the instantaneous position of the corresponding material points and the instability core, the spectral norm of the instantaneous sensitivity tensor $I(x, y, t)$ is superposed to the closed trajectories. For both mode A and mode B, the high sensitivity regions strictly follow the movement of the material points along the orbits. This is probably more evident for mode B, which is characterized by a larger wavenumber k and is obtained for a larger Reynolds number.

These results suggest that it might be possible to describe the spatio-temporal evolution of the instability through a 'local theory'. A possibility in this sense could be offered by the inviscid short-wavelength approximation developed by Lifschitz & Hameiri (1991). A similar framework has been used to study both elliptic, hyperbolic

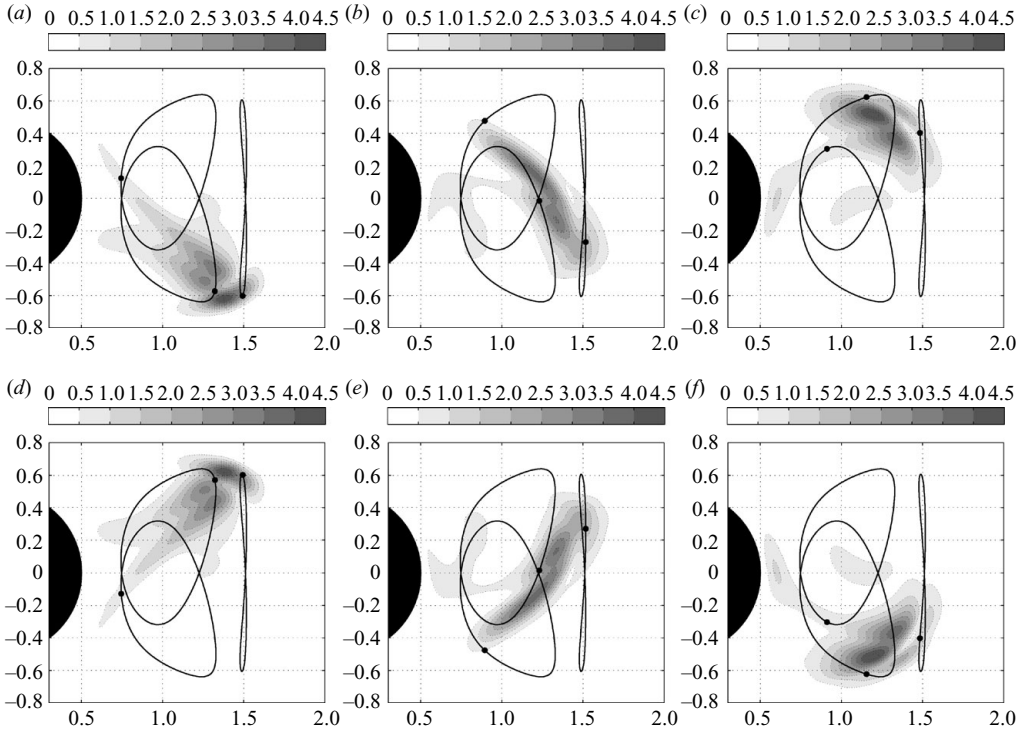

FIGURE 6. Closed Lagrangian trajectories of the periodic base flow at $Re = 260$: the movement of the points (small circles) along the closed orbits (black lines) is shown for (a–f) the six phases (0, $\pi/3$, $2\pi/3$, π, $4\pi/3$ and $5\pi/3$) in which the vortex -shedding cycle has been equally divided. The spectral norm of the sensitivity tensor $I(x, y, t)$ for mode B at $k = 7.64$) is also superposed in order to show the strong correlation existing among the orbits and the regions of instantaneous maximum sensitivity.

and centrifugal instabilities arising on top of stationary two-dimensional flows (see for instance Bayly 1988; Friedlander & Vishik 1991; Leblanc & Cambon 1998; Sipp & Jacquin 1998; Sipp, Lauga & Jacquin 1999 and Caulfield & Kerswell 2000). According to this theory, the solution of the LNSEs is sought in the form of a rapidly oscillating and localized wave packet. At leading order, for vanishing viscosity ($Re \to 0$) and large wavenumbers ($k \to \infty$), short wavelength instabilities propagate along Lagrangian trajectories. In such context, a special role can be ascribed to the closed Lagrangian trajectories previously described. On such orbits, in fact, the instability wave can feed back on itself giving rise to a self-excited oscillation.

A preliminary application of this theory along the three closed orbits has shown that the periodic flow in the wake of the cylinder is highly unstable with respect to short-wavelength perturbations. However, no quantitative agreement between the growth rates predicted by the asymptotic theory and those obtained by the global stability analysis has been found yet. Considering that for the cylinder wake the value of Re is only moderately large and that the values of k corresponding to the maximum amplification for both mode A and mode B are only slightly larger than one, it is clear that both finite Reynolds number and finite wavenumber effects might make a significant contribution to the global growth rate and therefore should be included in a quantitative and rigorous analysis. Furthermore, the theory should also

provide a way to build the spatial structure of the global mode starting from the local approximation along the orbits.

Landman & Saffman (1987) showed how to introduce in the leading order equations a term accounting for a viscous correction. Bayly (1988), on the other hand, showed that in the context of two-dimensional steady flows with closed streamlines, it is possible to build an inviscid global mode of finite wavenumber in the proximity of the most unstable orbit. For the cylinder case, however, a 'local theory' accounting for finite wavenumber effects and relating the characteristics of the Lagrangian orbits and the global behaviour of the self-sustained instability is still lacking (if any will ever be possible). At the present stage of development, thus, it is difficult to say something conclusive about the possibility to describe the instability by using a local approach and further investigations are necessary to clarify this point. In any case, there is a spatial resemblance between the sensitivity maps and the closed orbits which might lead to a future interpretation of the instability mechanism even if the short wavelength theory should turn out to be inapplicable.

REFERENCES

Barkley, D. 2005 Confined three-dimensional stability analysis of the cylinder wake. *Phys. Rev.* E **71**.

Barkley, D. & Henderson, R. D. 1996 Three-dimensional floquet stability analysis of the wake of a circular cylinder. *J. Fluid Mech.* **322**, 215–241.

Bayly, B. J. 1988 Three-dimensional centrifugal-type instabilities in inviscid two-dimensional flows. *Phys. Fluids* **31**, 56–64.

Bottaro, A., Corbett, P. & Luchini, P. 2003 The effect of base flow variation on flow stability. *J. Fluid Mech.* **476**, 293–302.

Brede, M., Eckelmann, H. & Rockwell, D. 1996 On secondary vortices in a cylinder wake. *Phys. Fluids* **8**, 2117–2124.

Caulfield, C. P. & Kerswell, R. R. 2000 The nonlinear development of three-dimensional disturbances at hyperbolic stagnation points: a model of the braid region in mixing layers. *Phys. Fluids* **12**, 1032–1043.

Chomaz, J.-M. 2005 Global instabilities in spatially developing flows: non-normality and nonlinearity. *Annu. Rev. Fluid Mech.* **156**, 209–240.

Davis, T. A. 2004 Algorithm 832: UMFPACK, an unsymmetric-pattern multifrontal method. *ACM Trans. Math. Software* **30** (2), 196–199.

Drazin, P. G. 2002 *Introduction to Hydrodynamic Stability*. Cambridge University Press.

Friedlander, S. & Vishik, M. M. 1991 Instability criteria for the flow of an inviscid incompressible fluid. *Phys. Rev. Lett.* **66**, 2204–2206.

Giannetti, F. & Luchini, P. 2007 Structural sensitivity of the first instability of the cylinder wake. *J. Fluid Mech.* **581**, 167–197.

Ince, E. L. 1926 *Ordinary Differential Equations*. Dover.

Karniadakis, G. E. & Triantafyllou, G. S. 1992 Three-dimensional dynamics and transition to turbulence in the wakes of bluff bodies. *J. Fluid Mech.* **238**, 1–30.

Landman, M. J. & Saffman, P. G. 1987 The three-dimensional instability of strained vortices in a viscous fluid. *Phys. Fluids* **30**, 2339–2342.

Leblanc, S. & Cambon, C. 1998 Effects of the Coriolis force on the stability of Stuart vortices. *J. Fluid Mech.* **356**, 353–379.

Lehoucq, R. B., Sorensen, D. C. & Yang, C. 1998 *ARPACK Users Guide: Solution of Large Scale Eigenvalue Problems by Implicitly Restarted Arnoldi Methods*. SIAM.

Leweke, T. & Provansal, M. 1995 The flow behind rings: bluff body wakes without end effects. *J. Fluid Mech.* **288**, 265–310.

Leweke, T. & Williamson, C. H. K. 1998 Three-dimensional instabilities in wake transition. *Eur. J. Mech.* **17**, 571–586.

Lifschitz, A. & Hameiri, E. 1991 Local stability conditions in fluid dynamics. *Phys. Fluids* **3** (11), 2644–2651.

Luchini, P., Giannetti, F. & Pralits, J. O. 2008 Structural sensitivity of linear and nonlinear global modes. In *Proocedings of the 5th AIAA Theoretical Fluid Mechanics Conference, June 23–26,* Seattle, Washington. *AIAA Paper* 2008-4227.

Marquet, O., Lombardi, M., Chomaz, J.-M., Sipp, D. & Jacquin, L. 2009 Direct and adjoint global modes of a recirculation bubble: lift-up and convective non-normalities. *J. Fluid Mech.* **622**, 1–21.

Marquet, O., Sipp, D. & Jacquin, L. 2008 Sensitivity analysis and passive control of cylinder flow. *J. Fluid Mech.* **615**, 221–252.

Mittal, R. & Balachandar, S. 1995 Generation of streamwise vortical structures in bluff body wakes. *Phys. Rev. Lett*. **75**, 1300–367.

Noack, B. R. & Eckelmann, H. 1994 A global stability analysis of the steady and periodic cylinder wake. *J. Fluid Mech.* **270**, 297–330.

Noack, B. R., König, M. & Eckelmann, H. 1993 Three-dimensional stability analysis of the periodic flow around a circular cylinder. *Phys. Fluids* A**5** (6), 1279–1281.

Rai, M. M. & Moin, P. 1991 Direct simulations of turbulent flow using finite-difference schemes. *J. Comp. Phys.* **96**, 15–53.

Sipp, D. & Jacquin, L. 1998 Elliptic instability in two-dimensional flattened Taylor-Green vortices. *Phys. Fluids* **10** (4), 839–849.

Sipp, D., Lauga, E. & Jacquin, L. 1999 Vortices in rotating systems: centrifugal, elliptic and hyperbolic type instabilities. *Phys. Fluids* **11** (12), 3716–3728.

Thompson, M. C., Leweke, T. & Williamson, C. H. K. 2001 The physical mechanism of transition in bluff body wakes. *J. Fluids Struct*. **15**, 607–616.

Williamson, C. H. K. 1988 The existence of two stages in the transition to three-dimensionality of a cylinder wake. *Phys. Fluids* **31**, 3165–3168.

Williamson, C. H. K. 1996*a* Three-dimensional wake transition. *J. Fluid Mech.* **328**, 345–407.

Williamson, C. H. K. 1996*b* Vortex dynamics in the cylinder wake. *Annu. Rev. Fluid Mech.* **28**, 477–539.

Zhang, H. Q., Fey, U. F. & Noack, B. R. 1995 On the transition of the cylinder wake. *Phys. Fluids* **7** (4), 779–794.

Zuccher, S., Luchini, P. & Bottaro, A. 2004 Algebraic growth in a blasius boundary layer: optimal and robust control by mean suction in the nonlinear regime. *J. Fluid Mech.* **513**, 135–160.